npj climate and atmospheric science

www.nature.com/npjclimatsci

ARTICLE OPEN

Check for updates

Transient vegetation degradation reinforced rapid climate change (RCC) events during the Holocene

Xinzhou Li[1]✉, Xiaodong Liu[1], Zaitao Pan[2], Zhengguo Shi[1], Xiaoning Xie[1], Hongyan Ma[1], Jizhou Zhai[1,3], Heng Liu[1,3], Xiaoxun Xie[1] and Aona Dai[1]

High-resolution multi-proxies from geological archives have revealed a series of rapid climate change (RCC) events during the Holocene. These events coincided with the so-called "Bond events", which were previously linked to a weakened thermohaline circulation. However, the proposed atmosphere-ocean teleconnections associated with these events are regionally distinct, which explains why most previous studies have only explained a subset of the RCC events, depending on region and proxy type; moreover, the suggested mechanisms are much debated. Here, we present a major effort of Holocene transient simulations that identify a series of centennial-scale RCC events that are consistent with records from geological archives. All eight Holocene RCC events were captured in North China (NC) and pervasive throughout the Northern Hemisphere (NH) in experiments with active dynamic vegetation modules (DV), whereas they were largely absent in experiments without DV. These results suggest that the collapse of the terrestrial vegetation and the resulting feedback played a crucial role in RCC events. Our findings supplement or even challenge the notion that North Atlantic cooling, closely linked to ice-rafted debris (IRD) events, was the dominant driver of RCC events.

npj Climate and Atmospheric Science (2023)6:125 ; https://doi.org/10.1038/s41612-023-00457-5

INTRODUCTION

The climatic evolution of the Holocene (11,700 years ago to the present) is closely related to the development of human civilization. As a somewhat representative interglacial period, the Holocene appears as an interval of overall relatively warm and stable climate; however, on finer temporal scales, the climate was frequently interrupted by multiple rapid climate change (RCC) events when precipitation and temperature fell sharply. Bond et al.[1] documented eight cold events based on records of ice-rafted debris (IRD) in North Atlantic deep-sea sediments, which are dated to 11.1, 10.3, 9.4, 8.1, 5.9, 4.2, 2.8, and 1.4 ka BP, respectively. Combined with two additional events at 7.2 ka BP[2,3] and the Little Ice Age at 0.4 ka BP (LIA)[4], the Holocene thus has a total of 10 RCC events. These events mostly lasted for decades or centuries[5–7], with a ~1500-year spacing[1,8]. Identifying the driving mechanism of these Holocene RCC events is of major theoretical and practical significance, given concerns about the societal impacts of ongoing climate change and possible future RCC events. Various proxy indicators and records have shown that the Holocene RCC events were not local but rather that they occurred throughout the Northern Hemisphere[9]. However, most of these proxy records document cold events at ~8.2 and ~4.2 ka BP[10–12], while other RCC events are less well-documented. In general, an RCC event was accompanied by cooling in high latitudes of the Northern Hemisphere, weakening of the tropical monsoon, and drying at low latitudes[13,14]. RCC events potentially increased the mortality rate amongst biological organisms and reduced their life expectancy, and they also had impacts on human population migration and agricultural production[15,16]. Cultural evolution in different parts of Eurasia was closely linked to RCC events which have been proposed as possible causes of the collapse of rain-fed agricultural systems and ancient civilizations, including the rise and fall of the Akkadian empire, the termination of the Harappan civilization in the Indus valley, and the collapse of the Liangzhu and Neolithic cultures in and around the Central Plain of China[17–20].

Most previous studies have linked Holocene RCC events to the Bond events and thus to the cooling of the North Atlantic[14] or to remote teleconnections[21], although regional differences exist[5,7]. The freshening of North Atlantic surface water and its relationship with the weakening of the North Atlantic Meridional Overturning Circulation (AMOC) is often invoked to explain global abrupt climatic events. However, skepticism has gradually emerged[22], including the fact that the 4.2 ka BP event was not associated with an injection of freshwater to the North Atlantic, as was found in a transient model simulation[23]. Thus, the origin of RCC events remains controversial, perhaps partly because of the neglect of the feedback of local surface environmental anomalies.

As a key component of terrestrial ecosystems, vegetation influences the exchanges of matter, energy, and momentum between the land and atmosphere via the effects of albedo, roughness, canopy conductivity, and leaf area[24,25]. Eight charcoal records from Europe show a clear link between Holocene fires, IRD events, and RCC events[26].

In the present study, we conducted four long-term transient experiments for the Holocene (see Methods and Table 1: Experimental design) using the Community Earth System Model (CESM1.2). These experiments were designed to evaluate the climatic effects of dynamic vegetation (DV), non-dynamic vegetation (nDV), orbital forcing (ORB), and vegetation forcing (VF). The transient DV experiment captured almost all RCC events since the early Holocene. According to geological records from East Asia, we named the eight RCC events as follows: the 9.2 ka, 8.2 ka, 7.2 ka, 5.2 ka, 4.2 ka, 2.6 ka, 1.2 ka, and LIA events. The durations of RCC events are roughly 200–500 years. Due to the limitations of the geological records and the neglect of high-latitude ice sheets[27],

[1]State Key Laboratory of Loess and Quaternary Geology, Institute of Earth Environment, Chinese Academy of Sciences, Xi'an, China. [2]Department of Earth and Atmospheric Sciences, Saint Louis University, St. Louis, MI, USA. [3]Xi'an Institute for Innovative Earth Environment Research, Xi'an, China. ✉email: lixz@ieecas.cn

Table 1. Experimental design.

Experiment names	Earth orbital parameters	Greenhouse gases	Dynamic vegetation	Model components
DV	Transient	Transient	Yes	All active
nDV	Transient	Transient	No	All active
ORB	Transient	Fixed at pre-Industrial	No	All active
VF	Fixed at pre-Industrial	Fixed at pre-Industrial	No, but terrestrial vegetation data are obtained from DV	The atmosphere and land are active, while the ocean and sea ice are fixed at pre-Industrial.

the rapid climate changes in the early Holocene (the 11.1 ka and 10.3 ka events documented by Bond et al.[1]) are not discussed here. Only the DV, among the four transient experiments, could reproduce a strong correspondence between Holocene proxy records and model simulations for all the eight RCC events, which suggests that the dynamic evolution of terrestrial vegetation and its feedback to climate may be a key factor generating these events.

RESULTS

RCC events in geological proxy archives and transient simulations

East Asia has abundant regional geological records, including those with high precision, accurate dating, and high continuity, and based on relatively unambiguous proxies. These records, which are derived, for example, from stalagmites[28] and pollen assemblages in lake sediments[29,30] and peats, have documented abrupt climatic events on centennial to millennial scales. However, these proxy records from different regions are often subject to limitations imposed by their environmental sensitivity and, thus, their fidelity in recording climatic changes. Consequently, previous studies have focused on only one or two RCC events that are recorded by a single proxy in a specific geographical region, except for the IRD events[1,2], which included multiple RCCs. A reconstruction of precipitation based on pollen analysis shows that the peak rainfall in the middle latitude of the East Asia region occurs during the early to mid-Holocene, followed by a significant decrease[29,31]. Stalagmite oxygen isotope ($\delta^{18}O$) with precise dating shows a more negative in the early Holocene and a less negative shift in the late Holocene, synchronizing with changes in summer solar radiation in the Northern Hemisphere[28,32]. Although the exact correspondence between oxygen isotope records and regional precipitation patterns and monsoon intensity in East Asia is not yet clear, long-term trends (on a millennial scale) and centennial-scale observations show that a more negative in oxygen isotopes corresponds to abundant rainfall, while a positive shift corresponds to dry periods[28]. We define Holocene RCC events in East Asia (see Methods section) by collating several high-resolution records from the East Asian region, combined with the subpolar North Atlantic hematite-stained grains (HSG, symbolically representing Bond events, Fig. 1a). It can be seen that RCC events given by the four geological records (Fig. 1b–e) in East Asia all well correspond to HSG. When the RCC events occur, HSG is roughly at the peak value with a slight timing shift.

Consistent with previous studies[31], we use the Holocene annual precipitation sequences in NC from the DV experiment for comparison with the geological records. It can be seen (Fig. 1f) that, with the dynamic feedback of the terrestrial vegetation, the DV experiment captured almost all eight Holocene RCC events that featured rapid precipitation declines. In all eight RCC events, precipitation decreased sharply at times that closely matched the geological records.

Typical detection methods for abrupt change in time series are often applied only to a limited number of series. In this study, the detection needs to be run over a global grid of 192×288 (latitude × longitude) sequences. Thus, a reliable yet efficient detection method of RCC events from both high-resolution geological indicators and model simulations is somewhat challenging computationally. To detect the Holocene RCC precipitation events simulated by the DV experiment, we choose the computationally simplistic KDJ index (see Methods: KDJ index) to test the abruptness of the annual precipitation change on a global scale. Compared to other general jump detection tests like the Kolmogorov–Smirnov test and specific tests like the one proposed by Bagniewski et al.[33], the KDJ index stands out for its effectiveness in detecting jumps with minimal instances of missing or false positives. Additionally, it demonstrates high efficiency, allowing us to apply it across a global grid with relative ease. The KDJ index revealed eight RCC drought events in NC that passed the chosen criteria (KDJ = 20, see Methods, Fig. 2b). The 10.3 ka event is also shown, although it is slightly above the threshold. The timings of the eight RCC precipitation events in NC are 9.14 ka, 8.14 ka, 7.26 ka, 5.1 ka, 4.22 ka, 2.62 ka, 1.20 ka, and 0.42 ka BP (Fig. 2b), and they are very consistent with the geological records (Fig. 1).

Relationship between RCC events and various forcing factors

Figure 2c, d respectively, show the annual precipitation and its KDJ index in NC produced by the nDV experiment. Although the nDV experiment did not simulate the long-term trend of Holocene precipitation[31], it still resulted in multiple centennial-scale climate oscillations. The KDJ index shows 5–6 rapid drought events, but only the 9.2 ka, 5.2 ka, 4.2 ka, and LIA events are consistent with the geological records, and the others were not detected. This may be because, in this case, the change in insolation caused by Earth orbital forcing is the main driver of precipitation changes across the East Asian monsoon region[28], and the annual precipitation series in NC from the ORB experiment shows synchronous changes with insolation. However, the KDJ index shows that only the 8.2 ka and 10.3 ka events were detected (Supplementary Fig. 3); the 9.2 ka event appears to be delayed and is manifested as an 8.95 ka BP event, and an extreme precipitation decline also occurred at 3.05 ka BP. These results suggest that Earth's orbital changes drove several of the RCC events during the Holocene[34]. By comparison, the Earth orbital forcing (ORB) and the combination of greenhouse gases (GHG) and Earth orbital forcing (nDV) experiments failed to capture all RCC events at the same time, or only 1–2 events.

The difference between the DV and nDV experiments shows that the dynamic vegetation feedback not only caused the mid-Holocene (7.8 ka BP) precipitation peak in NC, which was followed by a significant declining trend since the mid-Holocene[31] but, more importantly, also caused a rapid decrease in precipitation during almost all the RCC events (Fig. 2e). We performed empirical orthogonal function (EOF) analysis on the total terrestrial vegetation (TotalVeg) of East Asia from DV to find key sensitive areas and modes of vegetation response to climate change (Supplementary Fig. 2a, b). The variance contribution from the first three EOF in TotalVeg accounts for 33.3%, with the first one being 14.4%. In the middle portion of the Holocene, the time coefficient is positive with more vegetation in NC, while in the early and late

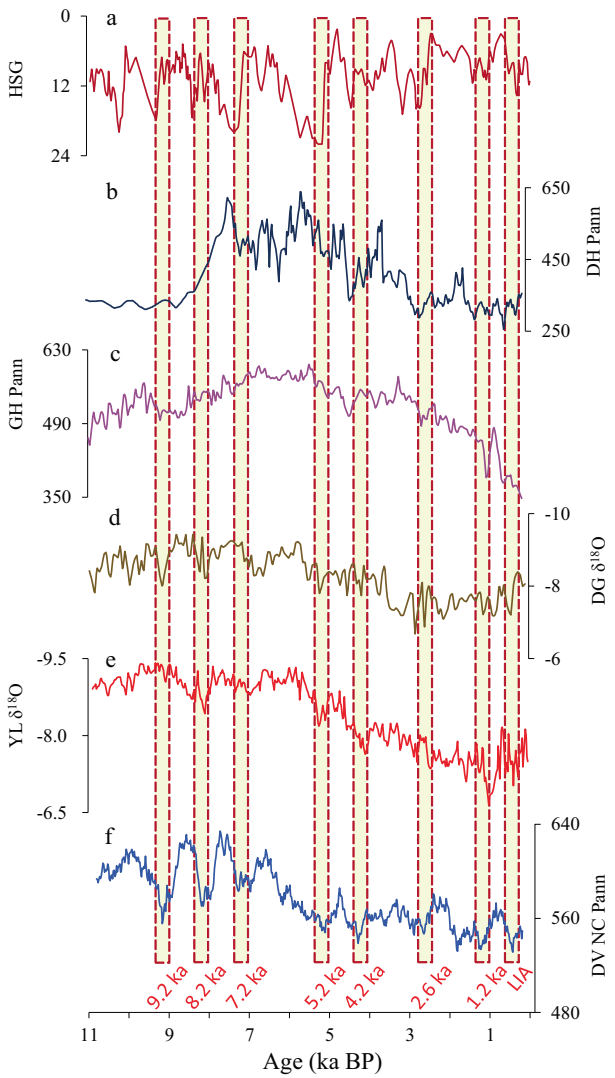

Fig. 1 Holocene rapid climate change (RCC) events. a Hematite-stained grain (HSG) from the subpolar North Atlantic (Bond et al., 2001) is used to represent Bond events. **b**, **c** Sequences of pollen-reconstructed annual precipitation (Pann) from Daihai (DH) and Gonghai (GH) lakes. **d**, **e** Stalagmite oxygen isotope ($\delta^{18}O$) records from Dongge (DG) and Yulong (YL) caves. **f** Pann in North China (NC) from the DV experiment. The eight yellow columns indicate the approximate ages of the Holocene rapid climate change (RCC) events (the same as below).

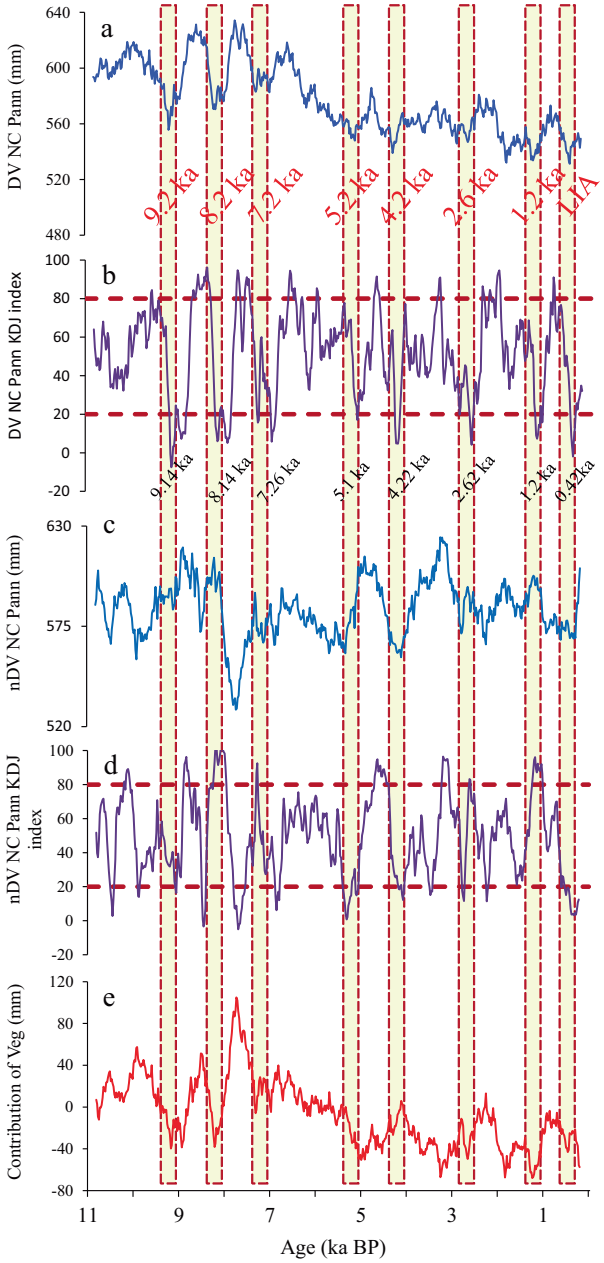

Fig. 2 Contribution of terrestrial vegetation to the Holocene RCC events in NC. a, **b** Annual precipitation over NC (same as in Fig. 1f, to facilitate comparison) and its KDJ index from the DV experiment; **c**, **d** annual precipitation in NC and its KDJ index from the nDV experiment; **e** contribution of vegetation anomalies (differences between DV and nDV) to precipitation. The bold red dotted lines indicated that the KDJ index values ≤20 or ≥80 have passed the thresholds.

Holocene, the time coefficient is negative with less vegetation. This indicates that the dry-wet transition area in East Asia is a sensitive area of Holocene vegetation change, also known as the key area. The relationship between TotalVeg and precipitation was further analyzed by Singular Value Decomposition (SVD), and their leading modes were shown in Supplementary Fig. 2c–e. The correlation between the time coefficients of TotalVeg and precipitation (Pann) for the first three pairs of singular value vectors of precipitation are 0.62, 0.58, and 0.62, respectively, exceeding the significance level of 0.01. The variance contributions from the first three modes are 16.75, 12.92 and 10.51%, respectively. Vegetation and precipitation change in East Asia have apparent coupling modes and synchronous variability (Supplementary Fig. 2c–e).

During the 9.2 ka, 8.2 ka, and 2.6 ka events, the annual precipitation in DV decreased by nearly 40 mm compared with nDV. The mid-Holocene precipitation in NC was generally higher than pre-industrial, but during the 7.2 ka event, the surface vegetation feedback also caused the precipitation to decrease by nearly 5.9 mm. The strongest vegetation effect occurred during the 5.2 ka and 1.2 ka events when the precipitation decreased by 50.66 and 67.96 mm, respectively, and during the 4.2 ka and LIA events, when the annual precipitation in NC decreased by 26.78 and 43.1 mm, respectively (Fig. 2e). Therefore, we now focus on a comparative analysis of the influence of the dynamic evolution of the terrestrial vegetation and its feedbacks on the RCC drought events during the Holocene, including their global distribution.

Contrasting the DV with nDV and ORB experiments, the latter two without vegetation dynamic feedback can also produce a few of the eight RCC events. The nDV captured 9.2 ka, 5.2 ka, 4.2 ka, and LIA with some timing offset (Fig. 2), and ORB simulated only 8.2 ka correctly (Supplementary Fig. 3). Further inspection shows that these RCC events are generally stronger than those missed ones (7.2 ka, 2.6 ka, and 1.2 ka), which seems to indicate that the dynamic vegetation feedback can help capture those weaker RCC events that would be missed otherwise. Furthermore, dynamic vegetation feedback corrects the timing of all RCC events to be consistent with the geological proxies.

Contribution of the terrestrial dynamical vegetation to RCCs

Vegetation abundance has three main effects on temperature: via changes in albedo, transpiration efficiency, and surface roughness. Vegetation can have both warming and cooling effects depending on geographical location. For example, in the warm and moist tropics, the abundant vegetation greatly increases transpiration and cools the environment; and in the cold and dry middle and high latitudes or the wet-dry transitional zone, the albedo effect dominates, and vegetation abundance (degradation) has a warming (cooling) effect. The abrupt collapse and migration of terrestrial ecosystems are not only the result of climate change, but they also have a strong feedback effect on climate[25,35]. The terrestrial vegetation, as a key factor in land-atmosphere exchange, has a complex two-way feedback relationship with the atmosphere. Charney[36] conducted the first project to document a significant positive feedback relationship between a vegetation anomaly and precipitation in Saharan Africa. Subsequently, an increasing number of studies focused on the interaction between climate and vegetation[37–39].

Figure 3a shows the TotalVeg sequence in the arid and semi-arid region of NC (defined as the area with >10% bare land at the present day in the DV experiment). Corresponding to the precipitation decrease, the vegetation percentage during almost every drought event is at a minimum, from which we infer that the dynamic evolution of the terrestrial vegetation was a prerequisite for rapid changes in precipitation during the Holocene.

To demonstrate the modulation of Holocene RCC events by the terrestrial vegetation, we conducted a VF experiment in which surface vegetation data were "imported" from DV, while other forcings (GHGs and the Earth orbital configuration) were fixed (see Table 1 and Methods). Except for the absence of the 9.2 ka event and the likely delay of the 2.6 ka event to 2.3 ka BP[40], the VF experiment also accurately reproduced the six other RCC events. The VF results confirm that the precipitation during the 8.2 ka, 7.2 ka, 5.2 ka, 4.2 ka, 1.2 ka, and LIA events decreased by 20.16, 8.4, 23.45, 35.15, 8.99, and 22.02 mm, respectively (see Supplementary Dataset 1), due solely to the degradation of the terrestrial vegetation. Although the 2.6 ka event was not simulated, the lowest precipitation value of the entire Holocene simulated by VF was at 2.3 ka BP, when the annual precipitation decreased by 48.25 mm. The KDJ index also shows that these rapid drought events are statistically above the selected criteria (Fig. 3c). By analyzing the long-term change of each plant functional type (PFT) conducted by the DV experiment, we found that since the early Holocene, the terrestrial vegetation in NC underwent an obvious replacement[31], and the proportion of the vegetation was low during the RCC events (Fig. 3a and Supplementary Fig. 4). Clearly, the rapid precipitation reduction events were associated with vegetation degradation due to its feedback to climate. Using temperate broadleaf deciduous shrub (TempBDS) that is more sensitive in NC as an example (Supplementary Fig. 4a), during the 9.2 ka, 7.2 ka, 4.2 ka, 1.2 ka, and LIA events, the TempBDS representation is at a low level, with the minimum value occurring at ~2.3 ka BP. Although TempBDS is not a dominant vegetation type, its and others' combined contribution toward the total

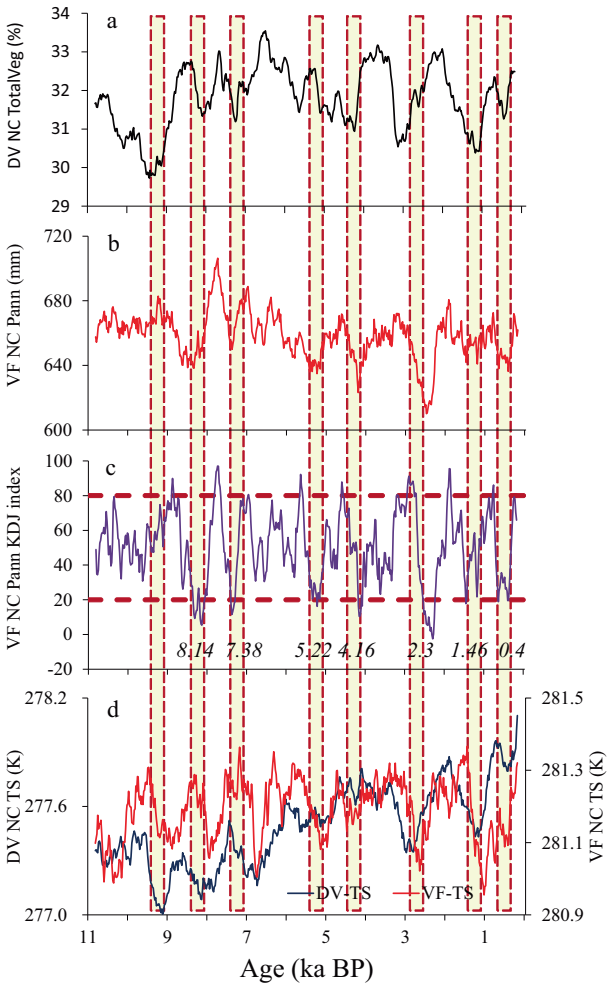

Fig. 3 Effects of terrestrial vegetation on annual precipitation (Pann) and surface temperature (TS) over NC during the Holocene. a Percentage of total surface vegetation (TotalVeg) from the DV experiment; **b**, **c** VF precipitation and its KDJ index; **d** TS for the DV and VF output. The bold red dotted lines indicated that the KDJ index values ≤20 or ≥80 have passed the thresholds.

vegetation coverage dwindling causes the surface albedo to increase and thus cool during RCC events. The close similarity of the DV and VF results further confirms the conclusion that the abrupt decreases in precipitation during the Holocene were associated with the feedback of rapid vegetation degradation to the climate system.

In terms of radiative processes, the vegetation degradation during the RCC events within the wet-dry transitional zone can cool the surface due to the increasing albedo[38,41]. In the DV experiment, the Holocene surface temperature (TS) sequence for NC captured almost all the drought events that corresponded to cooling (Fig. 3d), although the increasing trend since the early Holocene remains controversial[32]. The results of the VF experiment (Fig. 3d) also showed similar characteristics for all the RCC events except for the 7.2 ka event. The vegetation degradation has an obvious negative correlation with the surface albedo (Supplementary Fig. 5a), with the land surface albedo increasing when the vegetation cover decreases (Fig. 3a and Supplementary Fig. 5a). In terms of non-radiative processes, vegetation degradation can reduce evapotranspiration, resulting in an increase in sensible heat and a decrease in latent heat (Supplementary Fig. 5b), causing anomalous energy exchanges between the surface and atmosphere[31,42]. For example, forest loss in the Amazon region

since 2000 has dried the lower atmosphere, reduced water circulation, and led to increased drought severity and frequent fire outbreaks[43]. The partitioning between the sensible heat and latent heat flux can be characterized by the Bowen ratio, which is the ratio of sensible heat flux to latent heat flux. A larger Bowen ratio indicates that sensible heat is the dominant turbulent heat flux (Supplementary Fig. 5c), usually accompanied by a dry climate and even frequent fires. In contrast, the dominance of latent heat is accompanied by a humid climate. Supplementary Fig. 5b shows the surface sensible heat and latent heat fluxes in NC during the Holocene. Since the early Holocene, the sensible heat fluxes show a significant upward trend associated with a decrease in precipitation[31]. The Bowen ratio sequence (Supplementary Fig. 5c) shows a clear trend of increasing drying since the early Holocene, with the Bowen ratio peaking locally during each RCC event. The sequence of surface evaporation (Supplementary Fig. 5c) shows the opposite pattern to that of the Bowen ratio. Since the early Holocene, surface evaporation has decreased continuously, with rapid decreases during RCC events.

The annual surface temperature series in NC extracted from the DV experiment shows that, except for the 7.2 ka event, the land surface temperature also fell when the precipitation decreased rapidly (Fig. 3d). The annual surface temperature series in the DV and VF experiments (Fig. 3d) show that this cooling may be caused by terrestrial vegetation degradation. The above analysis indicates that the dynamic evolution of terrestrial vegetation is a key internal feedback process for the sudden decreases in precipitation and temperature during the Holocene. During the Holocene, the dynamic evolution of the terrestrial vegetation not only caused the long-term trend of precipitation decrease in NC during the Holocene, but it also played the dominant role in almost all the RCC events.

Global distribution of RCC events

Most geological records show that the RCC events in the Holocene were universal[7,10,11], which is confirmed by geological records and numerical simulations of a single event[23]. Supplementary Fig. 6 shows the annual precipitation and temperature sequences in the Northern Hemisphere (NH, 0–360°E, 0–80°N) and the Southern Hemisphere (SH, 0–360°E, 0–80°S). Clearly, the precipitation and temperature series in the NH share similar characteristics to those in NC, while they are different in the SH, which may be related to the different internal responses caused by the land and sea distribution and seasonal differences in insolation in both hemispheres[23]. Therefore, we extended the spatial extent of the RCC events from NC to NH. The Holocene annual precipitation series in NH shows a decreasing trend that tracks the decrease in summer insolation, while the global (land + ocean) and land precipitation decreased rapidly during all the RCC events, reaching a minimum. However, the nDV experiment (without vegetation dynamics) only showed low precipitation values during the 8.2 ka, 4.2 ka, and 1.2 ka events (Supplementary Fig. 7a). The nDV experiment gives higher annual precipitation in NH than the DV experiment, just the opposite of NC, which may be caused by other components of CESM rather than vegetation module, which is out of the scope for this study and will be studied in the future. The ORB experiment failed to capture any drought events (Supplementary Fig. 7c) and also showed a downward trend of Holocene precipitation in the Northern Hemisphere and a slightly enhanced precipitation signal around the mid-Holocene (Supplementary Fig. 7c), suggesting that the solar radiative forcing caused by Earth orbital changes was the main factor driving the long-term evolution of Earth's climate on the scale of the entire Holocene.

Like NC, the NH and SH temperature series for the Holocene obtained in the DV experiment show a rising trend since the mid-Holocene, while the temperature series in the NH show rapid reduction during all the RCC events (Supplementary Fig. 6b). However, in the nDV experiment (Supplementary Fig. 7b), there was no simultaneous cooling (cooling only occurred in the 1.2 ka event in the nDV experiment), and in the ORB experiment (Supplementary Fig. 7d) only the 2.6 ka event showed cooling. The general absence of cooling in the nDV and ORB experiments suggests also that the simultaneous decrease in temperature during the RCC events in the NH is closely related to the dynamic evolution of the vegetation and its feedback to climate.

RCC events in the Holocene have been detected by various proxy indicators in different regions worldwide. However, due to different geographical locations and internal feedback mechanisms, as well as the limitations of individual proxies, there are differences in their onset, duration, and relative amplitude of RCC events among different regions. Figures 4–5 and Supplementary Fig. 8 show the distribution of global precipitation, TotalVeg, and temperature anomalies of eight Holocene RCC events and multiple (all) RCC events ensemble (MRE) defined by regional proxy indicators in East Asia. The percentages of precipitation in RCC events (Methods) show that precipitation decreased in most regions of NH during almost all the RCC events. In addition to the sporadic precipitation on the Iranian Plateau and in the arid region of North Africa during the 5.2 ka and 7.2 ka events, the precipitation from East Asia to Central Asia, North Africa, and from central to southern North America was extremely low during all the RCC events. For example, the DV experiment showed that during the 9.2 ka, 8.2 ka, 2.6 ka, and 1.2 ka events, precipitation from North Africa to the Iranian Plateau was more than 30% less than what it was previously. When RCC events occur, the abnormal distribution characteristics of TotalVeg (Fig. 5) are very similar to that of precipitation. Precipitation anomalies from the VF experiment also have similar characteristics (Supplementary Fig. 9). During the 8.2 ka, 7.2 ka, 4.2 ka, 2.6 ka, 1.2 ka, and LIA events, the precipitation from Central Asia to North Africa and in southern North America was extremely low (Supplementary Fig. 9).

The annual mean surface temperature anomalies from the DV experiment during all the RCC events (Supplementary Fig. 6) also showed cooling over much of NH. In events 9.2 ka, 8.2 ka, and 7.2 ka, the temperature decreased in NC and Central Asia (Supplementary Fig. 8), while during events 5.2 ka, 4.2 ka, 2.6 ka, 1.2 ka, and the LIA, the temperature decreased across subtropical Asia. The North American continent also experienced a cooling in almost all RCC events, mainly in middle latitudes during the early to the mid-Holocene, with the cooling moving to lower latitudes in the late Holocene. This cooling shift from high to low latitudes during the Holocene may be related to the anomalous forcing of insolation caused by Earth's orbital changes, which will be discussed in a future paper. The distribution characteristics of cooling caused by the sole effect of vegetation forcing in the VF experiment (Supplementary Fig. 10) are like the DV results. Evidently, the degradation of the terrestrial vegetation contributed greatly to the decreases in precipitation and temperature across a large area of the NH during the Holocene RCC events.

Ignoring forcing by North Atlantic cooling

It should be noted that all the transient experiments in this study employed a 20-year acceleration technique, which means that the energy exchange between the sea surface and the deep ocean could not be truly reflected[11]. In addition, high-latitude ice sheets were fixed at the pre-Industrial value, ignoring its dynamic evolution (e.g., via iceberg calving) and its close association with North Atlantic cooling events[2,23,44,45]-which may be the main reason why the 11.1 ka and 10.3 ka Bond events[27] were not captured in the DV experiment. We calculated the NH sea surface temperature (SST) and Atlantic Multi-decadal Oscillation (AMO)-like features[23] from the DV experiment (Supplementary Fig. 11) to explore the relationship between the NH SST and North Atlantic SST anomalies and the Holocene RCC events[46].

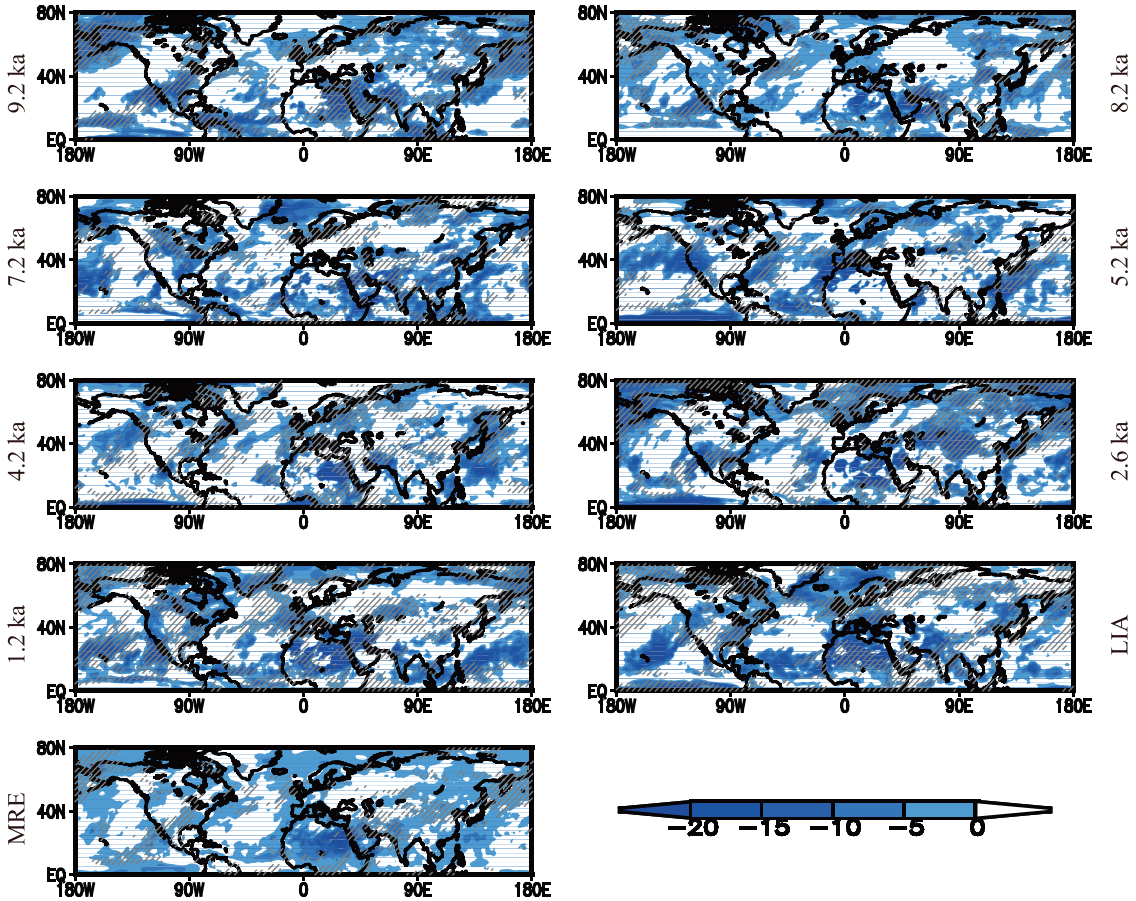

Fig. 4 Percentages of annual precipitation (unit: %) changes in eight RCC events and multiple (all) RCCs ensemble (MRE) during the Holocene from the DV experiment. The gray slanted lines indicated that the KDJ index had passed the thresholds (≤20).

Unfortunately, the NH SST and AMO-like sequences do not show all the RCC events of the Holocene. The NH annual, winter (December to February, DJF), and summer (June to August, JJA) SST and AMO-like features were at their lowest levels during the 2.6 ka, 1.2 ka, and LIA events, while the North Atlantic SST during the early to middle Holocene showed peak values during the 9.2 ka, 8.2 ka, 7.2 ka, 5.2 ka, and 4.2 ka events. There were no significant cooling events, such as at 9.2 ka, 5.2 ka, and 4.2 ka, in the Trace21 experiment[23,32]. Evidently, during the late Holocene (e.g., during the 2.6 ka, 1.2 ka, and LIA events), North Atlantic SSTs decreased, while during the early to mid-Holocene, the situation was more complicated. This suggests that the cooling of the North Atlantic during the early Holocene RCC events may have been related to the high-latitude ice sheet anomaly and the resulting freshwater injection, whereas this was not the case during the late Holocene. In addition, the occurrence of individual RCC events may be related to orbital or GHG forcing. Our DV experiment using the acceleration technique failed to simulate the Holocene cooling events over the North Atlantic, but it captured the Holocene RCC events, indicating that the dynamic evolution of the terrestrial vegetation and its feedback to climate is crucial in long-term climate evolution and in causing of RCC events. The IRD record[1,2] clearly points to rapid cooling in the North Atlantic during the Holocene RCC events. Combing all these observations, we suggest that the RCC events during the Holocene were the result of multiple factors and that the high sensitivity of the terrestrial vegetation to climate change on the region, scales-especially in arid and semi-arid regions where the vegetation dynamics and its feedback to climate are especially obviously- were a prerequisite for the RCC events.

DISCUSSION

In this study, we attempted to generalize all RCC events by conducting four transient Holocene numerical experiments with (DV) and without activating the dynamic vegetation (nDV) module. Convincingly, the DV experiment captured almost all the RCC events during the Holocene, while the other forcing experiments either failed or caught only a few events, such as the nDV experiment, which indicated that RCC events occurred at 9.2, 7.2, 5.2, 4.2 ka and LIA, and the ORB experiment only captured the 9.2 and 8.2 ka events. We conclude that insolation driven by Earth's orbital changes is a key external force that regulates the long-term evolution of precipitation during the Holocene. However, to better reproduce the Holocene rapid climate change events, the dynamic evolution of terrestrial vegetation and its feedback must be considered at the same time; otherwise, the simulations will fail or only catch a small percentage of RCC events.

A fundamental principle of ecology is that species must be able to adapt to the local climatic and environmental conditions for them to thrive at a given location. Climate change can affect the fitness and mortality of vegetation species. The feedback between vegetation and climate can be summarized as follows: when the main factors such as solar radiation, precipitation, and temperature transition from one equilibrium state to another, the response of vegetation to climate alters the competition relationship among different types of vegetation, and the proportion of individual vegetation is redistributed. These transient disturbances, manifested especially by differential changes in tree mortality, can lead to complex and sometimes unexpected changes in ecosystem composition, structure, and function[47]. Reduced rainfall and the

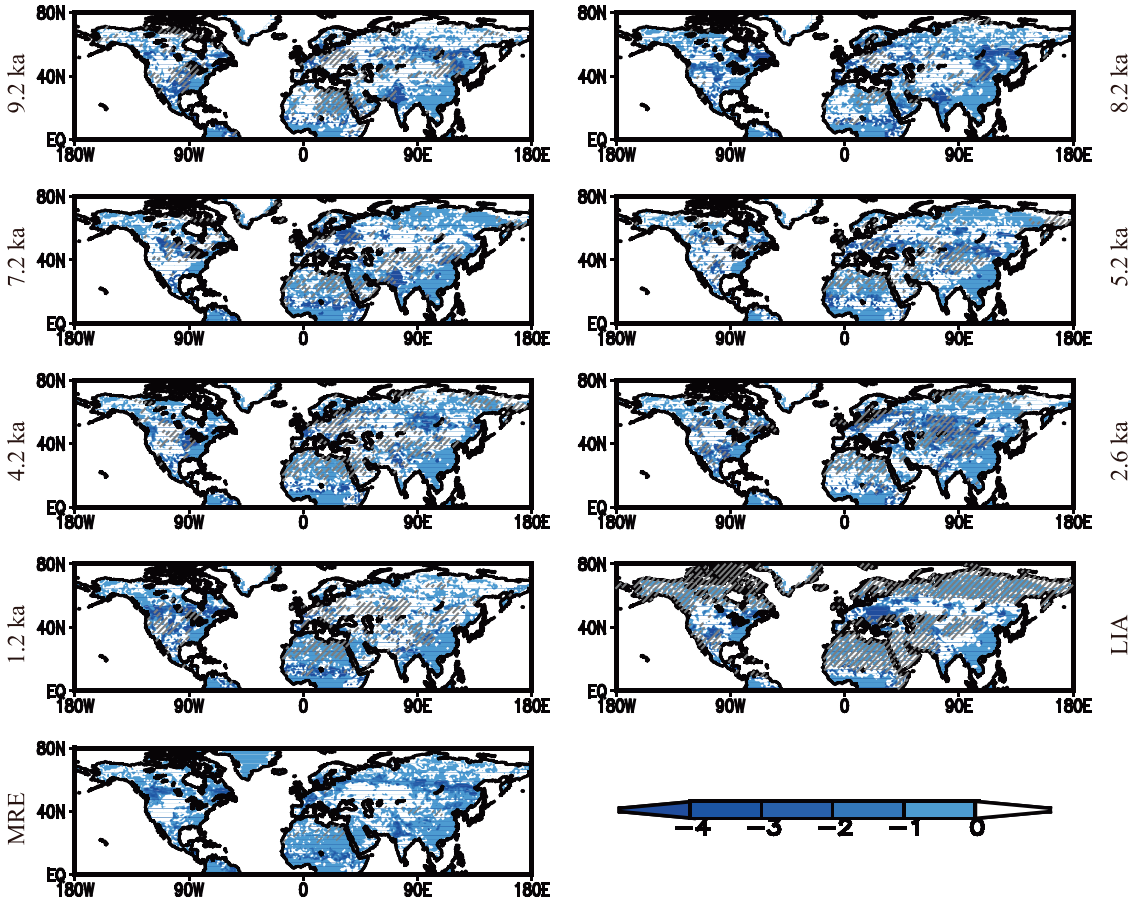

Fig. 5 Percentages of total vegetation (TotalVeg, unit: %) changes in eight RCC events and multiple (all) RCCs ensemble (MRE) during the Holocene from the DV experiment. The gray slanted lines indicated that the KDJ index have passed the thresholds (≤ 20).

increased frequency of drought enhance forest flammability and thus hinder forest growth. The vulnerability of vegetation across the arid and semi-arid transition zone determines its varying response to climate change[48]. At the same time, the rapid degradation of terrestrial vegetation will induce large changes in climate and environment[49], which may also cause feedback anomalies due to the delayed response to precipitation[40]. The vegetation feedback is particularly strong for the following reasons. First, deforestation or vegetation degradation increases the albedo and thus lowers the surface temperature in cold/dry middle and high latitudes where the RCC events tend to occur. Second, the rapid cooling and drying during the RCCs reinforce the vegetation albedo effect by suppressing the vegetation's transpiration efficiency. Third, RCC events occur in semi-arid regions, such as NC, where the vegetation is particularly susceptible to the impacts of climate change. This vulnerability contributes to the occurrence of rapid climate changes in these areas.

The onset, duration, end time, magnitude, and intensity of individual rapid climate change events during the Holocene and their underlying mechanisms are not discussed in detail here because we wish to consider all eight RCC events. Most studies have attributed the RCC events in the Holocene to changes in solar activity[2,50,51], high-latitude factors[52], interactions between the Northern and Southern Hemispheres, volcanic eruptions, and tropical ocean feedback- all of which are still debated. The dynamic evolution of terrestrial vegetation and its feedback may be another key factor, especially within the wet/dry transition region where the terrestrial vegetation is especially sensitive to climate change.

Although detailed analyses of a single or a couple of RCC events in different regions have been conducted, a single unified, unambiguous driving mechanism remains elusive. Moreover, a rapid climate change event may have completely different impacts in adjacent regions due to regional differences. For example, the Neolithic culture in North and South China collapsed at ~4 ka BP, while the Longshan culture in Central China flourished[30] at the same time. Pollen records from the Mediterranean[53] indicate the occurrence of several vegetation and climatic fluctuation events during the Holocene and the reconstructed precipitation series show that the timings of several RCC events across Europe were not consistent with those in East Asia. The 8.2 ka and 9.2 ka events in the geological record still differ greatly in terms of regional magnitude and intensity[34]. The timings of these RCC events in the Holocene vary between different regions, and their magnitude and intensity are also different; hence, these inconsistencies require additional numerical simulations and the careful comparison and validation of geological records.

METHODS

KDJ index

A variety of time series analysis methods can be used to detect the mutation characteristics of sequences[54]. In this paper, we calculate the KDJ index to detect the RCC events of the transient simulated Holocene climate series. The KDJ index was first proposed by George Lane[55] and has been widely used in analyzing stock market trends and change points. It can accurately find the lowest and highest point of a sequence[56]. Through comparative analysis of various methods, we found that the KDJ index could

decompose a sequence for several times to detect multiple time periods or time points with rapid changes. It is simple to calculate and has a low missing rate of change points. This is also the first attempt to apply this method to RCC research. In addition, through the decomposition of stock market series and climate change, such as precipitation series, we find that the "overbought" period in the stock market corresponds to the period of abundant precipitation or high temperature, while the "oversold" corresponds to the less precipitation or low temperature.

Here is an introduction to the KDJ index. The indicator generally consists of three lines (*K*, *D*, and *J*): K represents the fast confirmation line, *D* represents the slow main line, and *J* represents the direction-sensitive line (rapid change line). These three lines are based on the maximum, minimum, and current values in a certain period and are obtained by a specific calculation method. It first calculates the RSV value (Raw Stochastic Value) in a certain period, then calculates the *K*, *D*, and finally, the *J* values. The calculation formula is:

$$\mathrm{RSV}_n = ((C_n - L_m)/(H_m - L_m)) \times 100 \quad (1)$$

where RSV_n is the RSV value for the *n*th year, C_n is the *n*th year value. L_m and H_m are divided into *m*-year (period) minimum values and maximum values before the *n*th year. The value of *m* is related to the test period. In this study, we focus on RCC events from 100 to 1000 years, so m is set to 21 (~420 years).

$$K_n = (2/3) \times K_{n-1} + (1/3) \times \mathrm{RSV}_n \quad (2)$$

$$D_n = (2/3) \times D_{n-1} + (1/3) \times K_n \quad (3)$$

Here, K_{n-1} and D_{n-1} are the *K* and *D* values of the previous year, respectively. If there is no value in the previous year, the middle value of 50 is taken; thus, K_n and D_n of the current year are calculated.

Therefore, the KDJ index is obtained:

$$J_n = 3 \times K_n\text{-}2 \times D_n \quad (4)$$

The *K*, *D*, and *J* calculated by the above functions are closely linked, but they can also be used independently, in which the values of *K* and *D* range from 0 to 100, while the values of *J* can be ≥100 and ≤0. In terms of sensitivity from the perspective of climate change, *J* is the most sensitive, followed by *K*, and *D* is the least sensitive. The practical significance of a *J* value lies in finding the maximum and minimum of the curve ahead of K and D in a certain period[57]. *J* is widely used in business forecasting[56] and can be used as a sensitive indicator of rapid climate change in the short and medium term. In this study, the value of *J* is termed the KDJ index. Using Eqs. (1)–(4), we calculated the KDJ index value of the global grid during the Holocene and defined KDJ index values ≤20 or ≥80 as low and high thresholds, respectively[55,58].

Determination of RCC events

There are various RCC events on different time scales in the climate system. It is difficult to gain an overall perspective on all the RCC events in the Holocene from a single proxy record. In this study, we selected the previously published four proxy records of Northern China—two precipitation sequences from lacustrine pollen and two stalagmite records to show the RCC of the study area and to compare with the North Atlantic IRD records[2]. These proxy indicators include the reconstructed precipitation series of lakes Daihai (Fig. 1b, DH)[59] and Gonghai (Fig. 1c, GH)[29], and the oxygen isotope (δ18O) sequences of Dongge (Fig. 1d, DG)[28,29] and Yulong (Fig. 1e, YL)[60] caves.

Here, by comparing with Bond events, we can determine an RCC event using at least three proxy indicators from East Asia. In this way, we finally identified eight RCC drought events in East Asia during the Holocene: 9.2 ka (GH, DG, and YL), 8.2 ka (GH, DG, and YL), 7.2 ka (DH, GH, and YL), 5.2 ka (DH, GH, DG, and YL), 4.2 ka (DH, GH, DG, and YL), 2.6 ka (DH, GH, DG, and YL), 1.2 ka (DH, GH, DG, and YL) and the LIA (DH, GH, DG, and YL), and they were shown graphically with yellow columns in Fig. 1 and others.

Numerical modeling

The Community Earth System Model (CESM1.2) released by NCAR was used in this study[61]. CESM1.2 consists of four sub-modules: atmosphere, land, ocean, and sea ice, and a coupler. The four sub-modules and coupler versions used in this study are CAM4, CLM4, CICE4, POP2, and CPL7. CLM4 included a dynamic global vegetation module (DGVM) which was used to simulate transient changes in terrestrial vegetation[39]. The DGVM mainly comprises the following: (1) Simple division of biogeographic rules according to climatic characteristics. (2) Carbon and nitrogen cycle modules were introduced to trace biogeochemical processes during the simulation of biological growth and decay. (3) A top-down approach was used, and the concept of the average individual was used to improve computing efficiency. (4) To generalize vegetation dynamic processes on a global scale, the DGVM only outputs plant functional types (PFTs) rather than species. The DGVM displays surface changes via 16 PFTs and 1 barren ground. It reliably displays terrestrial vegetation photosynthesis, respiration, carbon allocation, plant establishment, growth, turnover, mortality, and competition among PFTs. Various components can be turned on or off to distinguish the characteristics of the long-term evolution of terrestrial vegetation and its interaction with climate[31]. In this study, the horizontal resolution of the atmospheric and land modules is 0.9°◊1.25° (latitude ◊ longitude), with 26 and 17 vertical layers, respectively. The horizontal resolution of the ocean and sea ice modules is 0.5°◊0.5°, and the vertical resolution of the ocean is 60 layers.

We conducted four Holocene transient experiments (Table 1). The first is the Holocene transient experiment with dynamic vegetation (DV). The DV experiment was carried out in two steps. Under the fixed boundary conditions of the Earth's orbital parameters and GHGs at the level of 14,000 years ago[31], the CESM1.2 first integrated continuously for 600 years to reach equilibrium so that the model can automatically generate suitable terrestrial vegetation from bare ground. We then employed the 20-year acceleration technology (1 model year = 20 calendar years) in which the orbital parameters and GHGs values were replaced with the 21st calendar year to conduct experiments for the last 14,000 years, covering the entire Holocene. The second experiment is the same as the first, but with the dynamic vegetation module turned off (nDV) during the entire numerical integration process; that is, the terrestrial vegetation type is fixed at the pre-Industrial. The third is the orbital forcing experiment (ORB), which is the same as nDV but with fixed GHGs at the pre-Industrial level. In the first three experiments, CESM1.2 employs a fully coupled module. In other words, the atmosphere, land surface, ocean, and sea ice modules are all dynamically interactive in the DV, nDV, and ORB experiments. The fourth is the vegetation forcing experiments (VF). Different from the first three experiments, the ocean and sea ice sub-modules of CESM1.2 in VF were fixed at pre-industrial values. The DGVM module is turned off in CESM1.2 in the VF, and the terrestrial vegetation was obtained from the DV. The terrestrial vegetation PFTs in the VF are renewed once per-model year, while other factors such as Earth orbital parameters, GHGs, sea surface temperature, and sea ice capacity data are fixed at pre-Industrial values.

Based on the above transient experiments, we can obtain Holocene climate changes under four experiments of different forcing factors, compare them with geological records to evaluate the simulation ability of CESM1.2 on Holocene RCC events and identify the possible influence of different forcing factors on RCC events through the comparison among the four transient experiments. The results of the DV experiment that considers

the most forcing factors can be compared directly with geological proxies. The nDV gives the forcing results of insolation and GHGs. The difference between DV and nDV highlights the role of dynamic changes in terrestrial vegetation. The ORB singles out the effects of changes in insolation caused by Earth's orbit. VF also isolates the influence of terrestrial vegetation anomaly on climate.

In Fig. 2b, the KDJ value detected by the annual precipitation series in NC output in DV is highly consistent with the RCC events defined by geological proxy indicators in this paper, indicating that the KDJ index can be used for RCC event detection. Moreover, the KDJ indices of each grid point can be calculated so that the temporal and spatial distribution characteristics of rapid climate change can be discussed, which is difficult to achieve by other methods. For clarity, when displaying the spatial distribution of individual RCC events, we choose the average change between the 200 years prior to the beginning and 200 years after the end of an RCC period.

DATA AVAILABILITY

All measured proxy indices and simulated data presented here are attached in the Supplementary Dataset 1 and will also be available in the East Asian Paleoenvironmental Science Database (https://doi.org/10.12262/IEECAS.EAPSD2023001). The data mainly include (1) the subpolar North Atlantic hematite-stained grains (HSG); (2) pollen-reconstructed annual precipitation from Daihai Lake (DH Pann); (3) pollen-reconstructed annual precipitation from Gonghai Lake (GH Pann); (4) stalagmite oxygen isotope records from Dongge cave (DG $\delta^{18}O$); (5) stalagmite oxygen isotope record from Yulong cave (YL $\delta^{18}O$); (6) annual precipitation in northern China (NC) from the DV experiment; and (7) percentage of the total surface vegetation (TotalVeg) from the DV experiment in NC.

CODE AVAILABILITY

The codes that support the findings of this study are available from the corresponding author on request.

Received: 23 April 2023; Accepted: 15 August 2023;
Published online: 23 August 2023

REFERENCES

1. Bond, G. et al. A pervasive millennial-scale cycle in North Atlantic Holocene and Glacial climates. *Science* **278**, 1257–1266 (1997).
2. Bond, G. et al. Persistent solar influence on North Atlantic climate during the Holocene. *Science* **294**, 2130–2136 (2001).
3. Bakker, P., Clark, P. U., Golledy, N. R., Schmittner, A. & Weber, M. E. Centennial-scale Holocene climate variations amplified by Antarctic Ice Sheet discharge. *Nature* **541**, 72–76 (2017).
4. Keigwin, L. D. The little ice age and medieval warm period in the Sargasso Sea. *Science* **274**, 1504–1508 (1996).
5. O'Brien, S. R. et al. Complexity of Holocene climate as reconstructed from a greenland ice core. *Science* **270**, 1962–1964 (1995).
6. Enzel, Y. et al. High-resolution Holocene environmental changes in the Thar Desert northwestern India. *Science* **284**, 125–128 (1999).
7. Wanner, H., Solomina, O., Grosjean, M., Ritz, S. P. & Jetel, M. Structure and origin of Holocene cold events. *Quat. Sci. Rev.* **30**, 3109–3123 (2011).
8. Bianchi, G. G. & McCave, I. N. Holocene periodicity in north Atlantic climate and deep-ocean flow south of Iceland. *Nature* **397**, 515–517 (1999).
9. Dansgaard, W. Ice core evidence of abrupt climatic changes. *Dordrecht*. (Reidel, The Netherlands, 1987) 223–233.
10. Alley, R. B. & Agustsdottir, A. M. The 8k event: Cause and consequences of a major Holocene abrupt climate change. *Quat. Sci. Rev.* **24**, 1123–1149 (2005).
11. Booth, R. K. et al. A severe centennial-scale drought in mid-continental North America 4200 years ago and apparent global linkages. *Holocene* **15**, 321–328 (2005).
12. Rohling, E. J. & Palike, H. Centennial-scale climate cooling with a sudden cold event around 8,200 years ago. *Nature* **434**, 975–979 (2005).
13. Thompson, L. G. et al. Kilimanjaro ice core records: evidence of Holocene climate change in Tropical Africa. *Science* **298**, 589–593 (2002).
14. Gupta, A. K., Anderson, D. M. & Overpeck, J. T. Abrupt changes in the Asian southwest monsoon during the Holocene and their links to the North Atlantic Ocean. *Nature* **421**, 354–357 (2003).
15. Haak, W. et al. Massive migration from the steppe was a source for Indo-European languages in Europe. *Nature* **522**, 207–211 (2015).
16. Damgaard, P. D. B. et al. 137 ancient human genomes from across the Eurasian steppes. *Nature* **557**, 369–374 (2018).
17. Weiss, H. & Bradley, R. S. What drives societal collapse? *Science* **291**, 609–610 (2001).
18. deMenocal, P. B. Cultural responses to climate change during the late Holocene. *Science* **292**, 667–673 (2001).
19. Zhang, H. W. et al. Collapse of the Liangzhu and other Neolithic cultures in the lower Yangtze region in response to climate change. *Sci. Adv.* **7**, 48 (2021).
20. Kathayat, G. et al. Protracted Indian monsoon droughts of the past millennium and their societal impacts. *Proc. Natl Acad. Sci. USA* **119**, e2207487119 (2022).
21. Routson, C. C. et al. Mid-latitude net precipitation decreased with Arctic warming during the Holocene. *Nature* **568**, 83–87 (2019).
22. Emile-Geay, J., Cane, M., Seager, R., Kaplan, A. & Almasi, P. El Nino as a mediator of the solar influence on climate. *Paleoceanography* **22**, PA3210 (2007).
23. Yan, M. & Liu, J. Physical processes of cooling and mega-drought during the 4.2 ka BP event: results from TraCE-21ka simulations. *Climate* **15**, 265–277 (2019).
24. Cao, M. K. & Woodward, F. I. Dynamic responses of terrestrial ecosystem carbon cycling to global climate change. *Nature* **393**, 249–252 (1998).
25. Bonan, G. B. Forests and climate change: forcings, feedbacks, and the climate benefits of forests. *Science* **320**, 1444–1449 (2008).
26. Florescu, G. et al. Holocene rapid climate changes and ice-rafting debris events reflected in high-resolution European charcoal records. *Quat. Sci. Rev.* **222**, 105877 (2019).
27. Cuffey, K. M. & Clow, G. D. Temperature, accumulation, and ice sheet elevation in central Greenland through the last deglacial transition. *J. Geophys. Res.* **102**, 26383–26396 (1997).
28. Wang, Y. J. et al. The Holocene Asian Monsoon: links to solar changes and North Atlantic climate. *Science* **308**, 854–857 (2005).
29. Chen, F. H. et al. East Asian summer monsoon precipitation variability since the last deglaciation. *Sci. Rep.* **5**, 11186 (2015).
30. Xiao, J. L. et al. The 4.2 ka BP event: multi-proxy records from a closed lake in the northern margin of the East Asian summer monsoon. *Climate* **14**, 1417–1425 (2018).
31. Li, X. Z. et al. Orbital-scale dynamic vegetation feedback caused the Holocene precipitation decline in northern China. *Commun. Earth Environ.* **3**, 257 (2022).
32. Liu, Z. Y. et al. The Holocene temperature conundrum. *Proc. Natl Acad. Sci. USA* **111**, E3501–E3505 (2014).
33. Bagniewski, W., Ghil, M. & Rousseau, D. D. Tipping points in the Climate System: automatic detection of abrupt transitions in paleoclimate records. *Chaos* **31**, 113129 (2021).
34. Fleitmann, D. et al. Evidence for a widespread climatic anomaly at around 9.2 ka before present. *Paleoceanography* **23**, PA1102 (2008).
35. Scheffer, M., Carpenter, S., Foley, J. A., Folke, C. & Walker, B. Catastrophic shifts in ecosystems. *Nature* **413**, 591–596 (2001).
36. Charney, J. G. Dynamics of deserts and drought in the Sahel. *Quart. J. R. Met. Soc.* **101**, 193–202 (1975).
37. Zeng, N., Neelin, J. D., Lau, K. M. & Tucker, C. J. Enhancement of interdecadal climate variability in the Sahel by vegetation interaction. *Science* **286**, 1537–1540 (1999).
38. Alkama, R. & Cescatti, A. Biophysical climate impacts of recent changes in global forest cover. *Science* **351**, 600–604 (2016).
39. Bonan, G. B. & Doney, S. C. Climate, ecosystems, and planetary futures: the challenge to predict lift in Earth system models. *Science* **359**, eaam8328 (2018).
40. Cheng, J. et al. Vegetation feedback causes delayed ecosystem response to east Asian summer monsoon rainfall during the Holocene. *Nat. Commun.* **12**, 1843 (2021).
41. Lee, X. et al. Observed increase in local cooling effect of deforestation at higher latitudes. *Nature* **479**, 384–387 (2011).
42. Duveiller, G., Hooker, J. & Cescatti, A. The mark of vegetation change on Earth's surface energy balance. *Nat. Commun.* **9**, 679 (2018).
43. Malhi, Y. et al. Climate change, deforestation, and the fate of the Amazon. *Science* **319**, 169–172 (2008).
44. Morrill, C., LeGrande, A. N., Renssen, H., Bakker, P. & Otto-Bliesner, B. L. Model sensitivity to North Atlantic freshwater forcing at 8.2 ka. *Climate* **9**, 955–968 (2013).
45. Matero, I. S. O., Gregoire, L. J., Ivanovic, R. F., Tindall, J. C. & Haywood, A. M. The 8.2 ka cooling event caused by Laurentide ice saddle collapse. *Earth Planet. Sci. Lett.* **473**, 205–214 (2017).
46. Shanahan, T. M. et al. Atlantic forcing of persistent drought in West Africa. *Science* **324**, 377–380 (2009).
47. Feeley, K. J. & Zuleta, D. Changing forests under climate change. *Nat. Plants* **8**, 984–985 (2022).
48. Berdugo, M., Gaitan, J. J., Delgado-Baquerizo, M., Crowther, T. W. & Dakos, V. Prevalence and drivers of abrupt vegetation shifts in global drylands. *Proc. Natl Acad. Sci. USA* **119**, e2123393119 (2022).

49. Ge, J. et al. Deforestation intensifies daily temperature variability in the northern extratropics. *Nat. Commun.* **13**, 5955 (2022).
50. Shindell, D. T., Schmidt, G. A., Mann, M. E. & Waple, A. Solar forcing of regional climate change during the Maunder Minimum. *Science* **294**, 2149–2152 (2001).
51. Steinhilber, F. et al. 9,400 years of cosmic radiation and solar activity from ice cores and tree rings. *Proc. Natl Acad. Sci. USA* **109**, 5967–5971 (2012).
52. Broecker, W. S. Does the trigger for abrupt climate change reside in the ocean or in the atmosphere? *Science* **300**, 1519–1522 (2003).
53. Combourieu-Nebout, N. et al. Holocene vegetation and climate changes in the central Mediterranean inferred from a high-resolution marine pollen record (Adriatic sea). *Climate* **9**, 2023–2042 (2013).
54. Aminikhanghahi, S. & Cook, D. J. A survey of methods for time series change point detection. *Knowl. Inf. Syst.* **51**, 339–367 (2017).
55. Lane, G. C. Lane's stochastics. *Stocks Commod.* **2**, 87–90 (1984).
56. Mizrach, B. & Weerts, S. Highs and lows: a behavioral and technical analysis. *Soc. Sci. Electron. Publ.* **19**, 767–777 (2008).
57. Amkraut, S., Girard, M. & Karl, G. Motion Studies for a work in Progress Entitled Eurythmy. *SIGGRARPH Video Rev.* **21**, 329–336 (1985).
58. Bai, Y. C., Yin, H. C. & Liu, S. J. Modified KDJ index based on wavelet analysis. *Elect. Sci. Tech.* **26**, 13–18 (2013).
59. Xu, Q. H., Xiao, J. L., Li, Y. C., Tian, F. & Nakagawa, T. Pollen-based quantitative reconstruction of Holocene climate changes in the Daihai lake area, Inner Mongolia, China. *J. Clim.* **23**, 2856–2868 (2010).
60. Bai, Y. J. et al. The multi-proxy record of a stalagmite from Yulong Cave, Hubei during the 4.2ka event. *Quat. Sci.* **40**, 959–972 (2020).
61. Hurrel, J. W. et al. The community earth system model: a frame-work for collaborative research. *Bull. Am. Meteorol. Soc.* **94**, 1339–1360 (2013).

ACKNOWLEDGEMENTS

This study was supported financially by the Chinese Academy of Sciences (CAS) Strategic Priority Research Program (XDB40030100), the National Natural Science Foundation of China (41991254), and the Science and Technology Innovation Project of Laoshan Laboratory (No. LSKJ202203300). We thank Professor J. Bloemendal at the University of Liverpool for the language improvement and X.X. Liu at the Institute of Earth Environment Chinese Academy of Sciences for helping to process the subpolar North Atlantic hematite-stained grains (HSG).

AUTHOR CONTRIBUTIONS

X.Z.L. designed the study, compiled the data, and wrote the paper. H.Y.M., J.Z.Z., and A.N.D. conducted the data analysis. X.D.L., Z.T.P., Z.G.S., X.N.X., H.L., and X.X.X. contributed to the data analysis, interpretation, and/or discussion.

COMPETING INTERESTS

The authors declare no competing interests.

ADDITIONAL INFORMATION

Supplementary information The online version contains supplementary material available at https://doi.org/10.1038/s41612-023-00457-5.

Correspondence and requests for materials should be addressed to Xinzhou Li.

Reprints and permission information is available at http://www.nature.com/reprints

Publisher's note Springer Nature remains neutral with regard to jurisdictional claims in published maps and institutional affiliations.